Su et al., http://www.jcb.org/cgi/content/full/jcb.201509085/DC1

Col18a1

Gene	HD	P Corr
Palld	0	0.65
Adamts1	0	0.62
Ctnna1	0	0.61
Lamb1	0	0.54
Pcolce	0	0.54
Fermt2	0	0.54
Nr2f6	0	0.53
Lmna	0	0.53
Lamb2	0	0.52
Kirrel	0	0.5
Smad6	0	0.49
Hspg2	0	0.49
Plod2	0	0.49
Tax1bp3	0	0.49
Tjp1	0	0.47
Mllt4	0	0.47
Vcl	0	0.47
Hoxb2	0	0.46
F11r	0	0.46
Ntn1	0	0.46
Pard3	0	0.46
Ntn4	0	0.45
Dlg5	0	0.45
Itgav	0	0.45
Tjp2	0	0.45
Wnt5a	0	0.44
Smo	0	0.43
Mylk	0	0.43
Adamts5	0	0.42
Wnt16	0	0.42
Rarg	0	0.42
Egfr	0	0.41
Erf	0	0.41
Sfrp1	0	0.41
Mfrp	0	0.41
C1qtnf5	0	0.41
Gpr126	0	0.41
Colec12	0	0.4
Lamc2	0	0.4
N2rf2	0	0.4

Col4a3

Gene	HD	P Corr
Col4a4	2	0.9
Cdh16	2	0.64
Ntn4	2	0.57
Tbx2	2	0.53
Pard6b	2	0.51
Lama3	2	0.48
Pax8	2	0.47
Smad6	2	0.41
Itgb6	3	0.6
Bmp6	3	0.56
Tspan18	3	0.4
Cfh	3	0.4
Shroom4	4	0.42
Gpr116	4	0.41
Lrp2	5	0.6
Npnt	5	0.55
Slc19a3	5	0.48
Igfbp7	5	0.44
Ace	5	0.44
Sema3g	5	0.43
Npr3	5	0.41
Oxgr1	6	0.53
Slc5a12	6	0.51
Scnn1b	6	0.44
Egflam	6	0.4
Pvrl3	7	0.49
Sftpb	7	0.45
Cgnl1	7	0.45
Trpv4	8	0.56
Slc5a10	8	0.46
Spon1	9	0.43
Umod	9	0.42
Veph1	10	0.65
Kcnj15	10	0.53
Kcnj1	10	0.48
Slc5a2	10	0.46
Scnn1a	10	0.4
Timp3	11	0.42
Crim1	12	0.47
Spry1	13	0.59

Col4a6

Gene	HD	P Corr
Fzd2	4	0.43
Fzd6	4	0.43
Col6a2	4	0.43
Col4a2	4	0.41
Sned1	4	0.41
Col4a5	5	0.64
Wnt5a	5	0.57
Lama3	5	0.54
Mylk	5	0.53
Pard3b	5	0.53
Lamc2	5	0.5
Lama2	5	0.5
Six5	5	0.49
Fat4	5	0.49
Palld	5	0.47
Hs3st3a1	5	0.47
Smo	5	0.47
Adamts1	5	0.47
Col16a1	5	0.46
Kirrel	5	0.45
Nr2f2	5	0.44
Casp14	5	0.44
Adamtsl4	5	0.43
Itga8	5	0.43
Fam46b	5	0.43
Pard3	5	0.43
Dsc2	5	0.42
Lamb2	5	0.42
Wnt16	5	0.42
Tbx22	5	0.41
Col17a1	5	0.41
Wnt4	5	0.41
Frem2	6	0.6
Tgfb3	6	0.47
Fat1	6	0.45
Fbln1	6	0.45
Cdh1	6	0.45
Tpm2	6	0.44
Col4a1	6	0.43
Tspan9	6	0.43

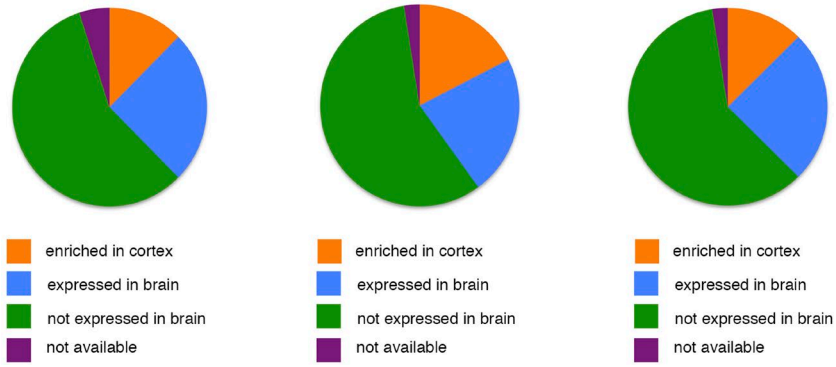

Figure S1. **Analysis of synaptogenic collagen genes with EvoCor.** Top genes predicted by EvoCor analysis as being functionally related to mouse *col18a1*, *col4a3*, and *col4a6* based on evolutionary history and tissue-wide gene expression patterns. HD, Hamming distance; PCorr, Pearson correlation. Tissue distribution of the 40 genes listed are shown in pie charts below each gene list. Only ~12% of *col18a1*, ~16% of *col4a3*, and ~12% of *col4a6* related top genes predicted by EvoCor analysis are enriched in mouse cortex.

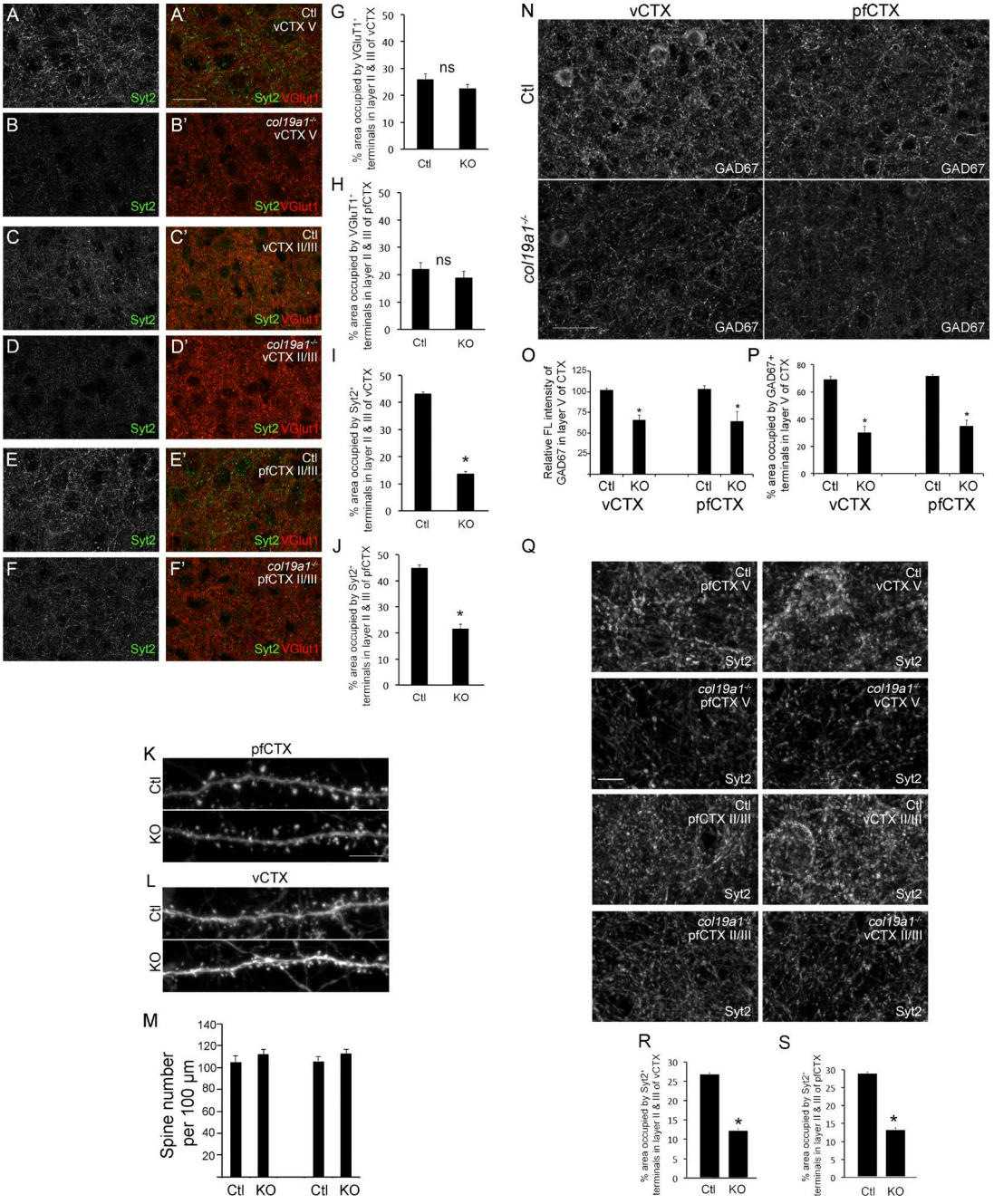

Figure S2. **Loss of collagen XIX leads to impaired inhibitory synapse formation.** (A–F) Immunostaining for Syt2 and VGluT1 in layer II/III and V of vCTX and pfCTX in P11 WT controls (Ctl) and *col19a1*$^{-/-}$ mutants. A–F depict Syt2 immunolabeling; A′–F′ depict merged overlay of Syt2 and VGluT1 immunolabeling. Bar, 25 µm. (G–J) Quantification of the area occupied by VGluT1 and Syt2 immunoreactivity in layer II/III of vCTX (M and O) and pfCTX (N and P) in P11 WT controls (Ctl) and *col19a1*$^{-/-}$ mutants. Data are mean ± SEM; *n* = 4. *, Differs from controls by P < 0.001 by Student's *t* test. ns, no statistical difference by Student's *t* test. (K and L) Dendritic spines were visualized in layer V pyramidal neurons in pfCTX and vCTX of *col19a1*$^{+/+}$*::thy1-yfp lineH* (Ctl) and *col19a1*$^{-/-}$*::thy1-yfp lineH* (KO) mice. Bar, 5 µm. (M) Numbers of dendritic spines per 100 µm were quantified in pfCTX and vCTX of *col19a1*$^{+/+}$*::thy1-yfp lineH* (Ctl) and *col19a1*$^{-/-}$*::thy1-yfp lineH* (KO) mice. Data are mean ± SEM; *n* = 3. ns, no statistical difference by Student's *t* test. (N) IHC for GAD67 in layer V of vCTX and pfCTX in P11 WT controls (Ctl) and *col19a1*$^{-/-}$ mutants. Bar, 40 µm. (O) Quantification of the relative fluorescent intensity of GAD67 immunoreactivity in layer V of vCTX and pfCTX in P23 control and KO. Data are mean ± SEM; *n* = 4. *, Differs from controls by P < 0.001 by Student's *t* test. (P) Quantification of the area occupied by GAD67 immunoreactivity in layer V of vCTX and pfCTX in P23 control and KO. Data are mean ± SEM; *n* = 4. *, Differs from controls by P < 0.001 by Student's *t* test. (Q) Immunostaining for Syt2 in layer II/III and V of pfCTX and vCTX in P56 WT controls (Ctl) and *col19a1*$^{-/-}$ mutants. Bar, 5 µm. (R and S) Quantification of the area occupied by Syt2 immunoreactivity in layer II/III of vCTX (R) and pfCTX (S) in P56 WT controls (Ctl) and *col19a1*$^{-/-}$ mutants. Data are mean ± SEM; *n* = 4. *, Differs from controls by P < 0.001 by Student's *t* test.

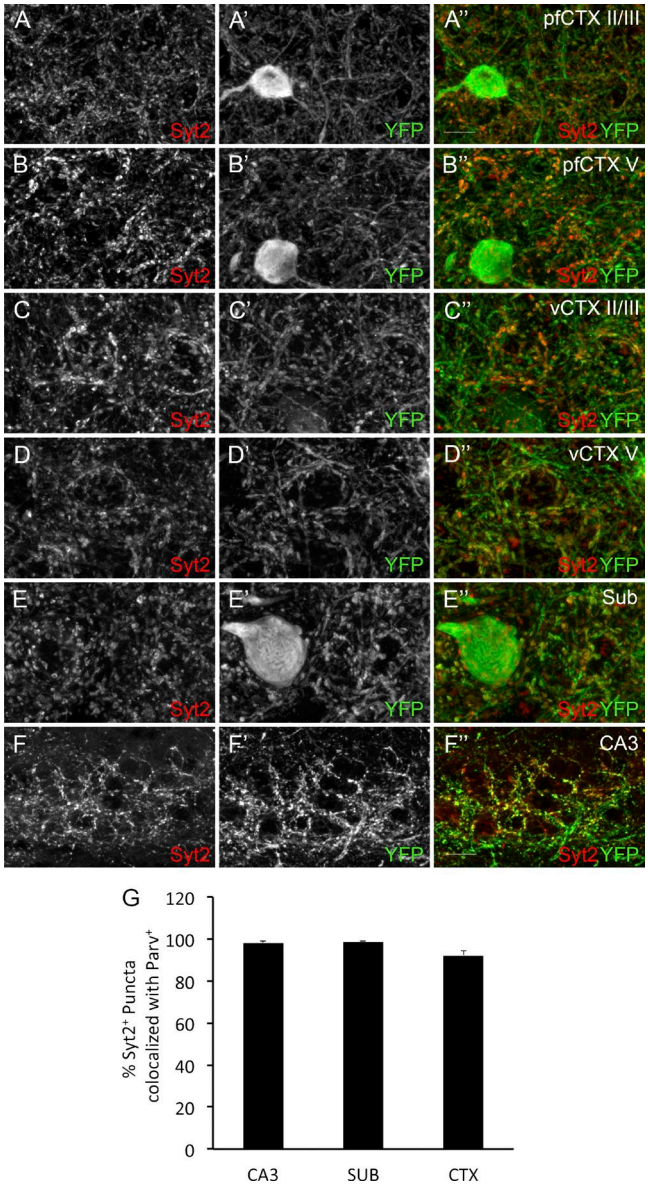

Figure S3. **Syt2⁺ terminals originated from Parv⁺ GABAergic interneurons in cortex and HP.** (A and B) Immunostaining for Syt2 in layer II/III (A) and layer V (B) of pfCTX in adult *parv-cre::thy1-stop-yfp* transgenic mice. A and B depict Syt2 immunolabeling; A′ and B′ depict YFP-*parv*; and A″ and B″ depict merged overlay of Syt2 immunolabeling and YFP-*parv*. Bar, 8 µm. (C and D) Immunostaining for Syt2 in layer II/III (C) and layer V (D) of vCTX in adult *parv-cre::thy1-stop-yfp* transgenic mice. C and D depict Syt2 immunolabeling; C′ and D′ depict YFP-*parv*; and C″ and D″ depict merged overlay of Syt2 immunolabeling and YFP-*parv*. (E) Immunostaining for Syt2 in subiculum of adult *parv-cre::thy1-stop-yfp* transgenic mice. E depicts Syt2 immunolabeling; E′ depicts YFP-*parv*; and E″ depicts merged overlay of Syt2 immunolabeling and YFP-*parv*. (F) Immunostaining for Syt2 in subiculum of adult *parv-cre::thy1-stop-yfp* transgenic mice. F depicts Syt2 immunolabeling; F′ depicts YFP-*parv*; and F″ depicts merged overlay of Syt2 immunolabeling and YFP-*parv*. Bar, 20 µm. (G) Quantification of the percentage of Syt2⁺ terminals in YFP-*parv* interneurons of CTX, subiculum, and CA3.

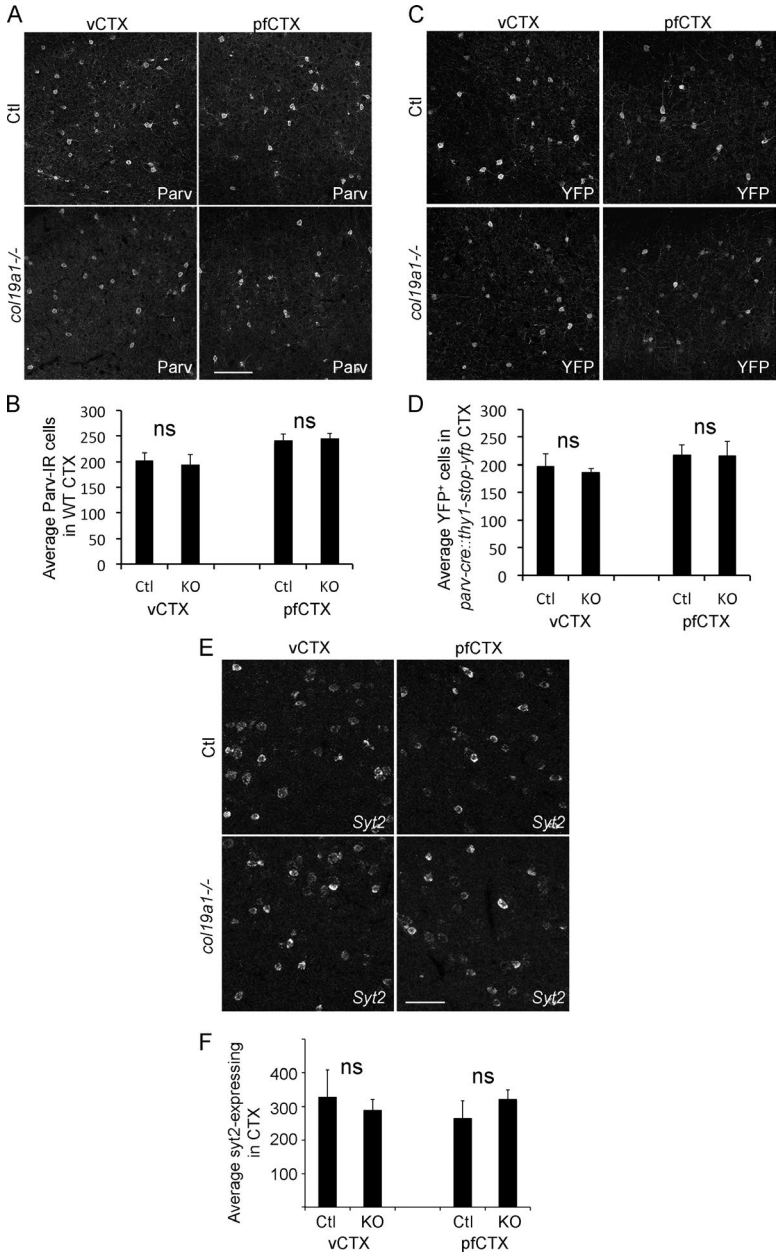

Figure S4. **Loss of collagen XIX does not alter the number or distribution of Parv⁺ or Syt2⁺ interneurons.** (A) Immunostaining for Parv in layer V of pfCTX and vCTX in P23 WT controls (Ctl) and *col19a1*$^{-/-}$ mutants (KO). Bar, 150 µm. (B) Quantification of the number of Parv⁺ cell bodies in pfCTX and vCTX of P23 control and KO. Data are mean ± SEM; *n* = 3. ns, no statistical difference by Student's *t* test. (C) Immunostaining for YFP in layer V of pfCTX and vCTX in P27 *parv-cre::thy1-stop-yfp* controls (Ctl) and *col19a1*$^{-/-}$*::parv-cre::thy1-stop-yfp* mutants (KO). (D) Quantification of the number of YFP⁺ cell bodies in pfCTX and vCTX of P27 control and KO (see C). Data are mean ± SEM; *n* = 3. ns, no statistical difference by Student's *t* test. Bar, 120 µm. (E) In situ hybridization for *syt2* mRNA in layer V of pfCTX and vCTX in P56 controls (Ctl) and *col19a1*$^{-/-}$ mutants (KO). Bar, 80 µm. (F) Quantification of the number of *syt2*⁺ cell bodies in pfCTX and vCTX of P56 control and KO (see E). Data are mean ± SEM; *n* = 3. ns, no statistical difference by Student's *t* test.

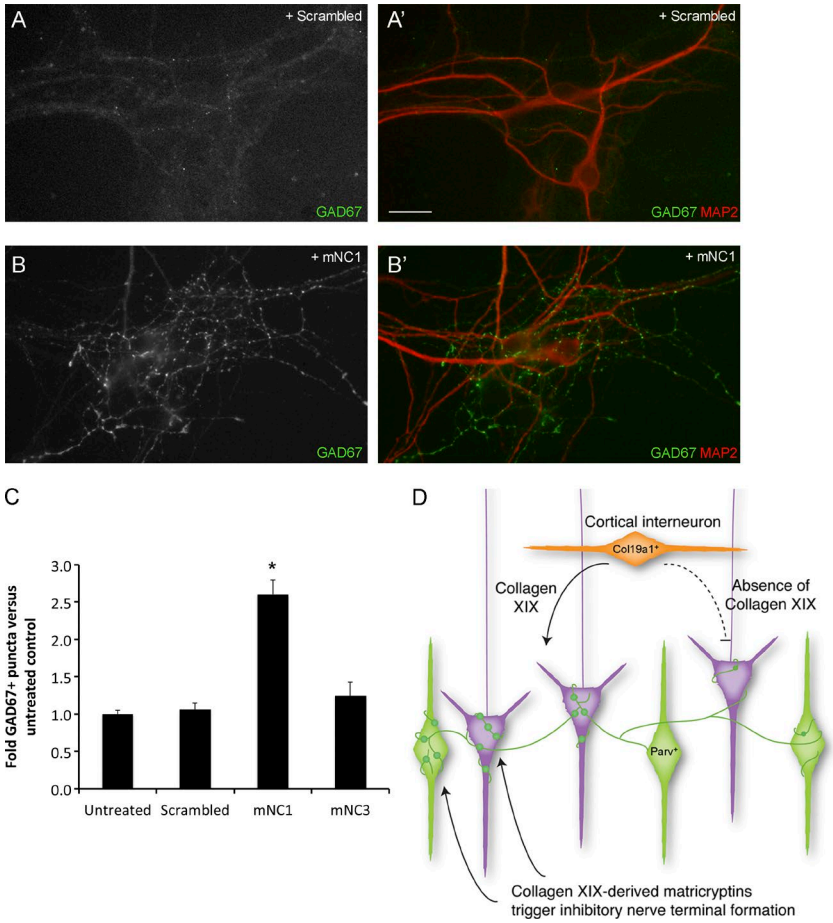

Figure S5. **In vitro application of mNC1 triggers an increase in GAD67+ puncta.** (A and B) Mouse NC1 (mNC1) triggers GAD67+ terminal formation. A and B depict GAD67 immunolabeling in HP cultures treated with Scrambled or mNC1 peptides; A′ and B′ depict merged overlays of GAD67- and MAP2-immunolabeling in these cultures. Bar, 20 µm. (C) Quantitation of mNC1-triggered GAD67+ puncta formation in HP neurons. Data are mean ± SEM; $n = 3$. *, Differs from controls, Scrambled, and mNC3 peptides by $P < 0.001$ by Tukey–Kramer test for difference between means. (D) Schematic depiction of the novel role for collagen XIX in Parv+ axosomatic synapse formation.